Journal of Hazardous Materials 174 (2010) 573–580

Contents lists available at ScienceDirect

Journal of Hazardous Materials

journal homepage: www.elsevier.com/locate/jhazmat

Facile fabrication of porous ZnO microspheres by thermal treatment of ZnS microspheres

Xiao Wu, KunWei Li, Hao Wang*

The College of Materials Science and Engineering, Beijing University of Technology, Beijing, 100124, PR China

ARTICLE INFO

Article history:
Received 20 August 2009
Accepted 16 September 2009
Available online 23 September 2009

Keywords:
ZnO
Porous microsphere
Photocatalytic properties

ABSTRACT

Porous ZnO microspheres with an average size of around 500 nm had been synthesized by thermal treatment of ZnS microspheres in an air atmosphere. The ZnS spheres had been synthesized at a low temperature of 100 °C by using L-cysteine (an ordinary amino acid) as a sulfur source with the assist of gelatin. By combining the results of X-ray diffraction (XRD), transmission electron microscope (TEM), field-emission scanning electron microscopy (FE-SEM), and Fourier transformation infrared spectra (FTIR), a structural and morphological characterization of the products was performed. The photocatalytic activity of ZnS microspheres and porous ZnO microspheres have been tested by degradation of Rhodamine-B (RB) under UV light, indicating that the porous ZnO microspheres showed enhanced photocatalytic performance compared to ZnS microspheres and commercial Degussa P25 TiO_2.

1. Introduction

Due to large surface area, high porosity and low density, porous materials are important functional materials which can be applied in the field of catalysis [1], sensor [2], luminescence [3], gas storage [4] and host–guest chemistry [5]. Porous semiconductor photocatalysts are attractive in applications such as bioengineering and photocatalysis, through minimizing the distance between the site of photon absorption and electron/hole redox reactions to improve efficiency [6]. The conventional method for porous material production involves the introduction of template molecules [7], directional freezing [8], ultrasonic spray pyrolysis [9] and so on. Recently, more and more attention has been attracted to the synthesis of porous materials because their different macroscopic morphologies are found to present different properties, which greatly affect their potential applications. For example, spherical porous particles and capsules have superiority in application for drug delivery and release [10,11]. However, except silica-based porous materials [10,11], there are few successful cases about precise control over the morphology of porous materials. Therefore, to explore a simple strategy for morphology controlled synthesis of porous materials is still a significant challenge for modern synthetic science.

ZnO is an important wide bandgap (3.37 eV) semiconductor with large exciton binding energy (60 meV) [12]. As one of the most attractive functional semiconductor materials, ZnO has been a focus of current research interest due to its promising applications in various fields, including short-wavelength light-emitting diode and room temperature ultraviolet (UV) lasing diode [13], solar cell [14], piezoelectric and optoelectronic device [15], UV-absorber [16], transparent conductor [17], field-emission display [18], gas sensor [19] and so on. In addition to this, it has also been demonstrated that ZnO has potential applications as a photocatalyst for the degradation of organic dyes [20]. It is well-known that the novel properties of materials are obviously dependent on crystallinity, crystal size, crystallographic orientation and morphology. Therefore, development of a morphologically controllable synthesis of ZnO semiconductor is urgently important to answer the demand for exploring the potential applications of ZnO [21]. Among diverse morphologies of ZnO, ZnO particles with a porous structure have attracted increasing attention in recent years since porous particles may present potential properties superior to corresponding solid structures. As far as we know, various porous ZnO structures, including porous pyramids [22], porous nanotubes [23], mesoporous polyhedral cages [24], porous hexagonal disks [25], porous nanowires [26] and porous nanobelts [27] have successfully prepared by means of various methods, but only a few cases have reported the synthesis of pure porous ZnO spheres[28,29].

In this paper, we report a simple and environmental friendly approach to fabricate porous 3D ZnO microspheres by thermal treatment of ZnS microspheres. The ZnS microspheres were synthesized via the reaction of $Zn(Ac)_2$ and L-cysteine ($C_3H_7NO_2S$,) in the presence of gelatin. It was found that the annealing temperature and time had obvious influence on the phase and morphology of the ZnO microspheres. The photocatalytic performance of ZnS micro-

* Corresponding author. Tel.: +86 10 67392733 fax: +86 10 67392445.
E-mail address: haowang@bjut.edu.cn (H. Wang).

0304-3894/$ – see front matter © 2009 Elsevier B.V. All rights reserved.
doi:10.1016/j.jhazmat.2009.09.090

spheres and porous ZnO microspheres were tested by degradation of Rhodamine-B (RB) under UV light.

2. Experimental

All the reagents were commercially available with analytical grade and used without further purification. In a synthetic process of ZnS, 1.0 g of granular gelatin (type B, 225 Bloom, from sigma) was dissolved in 30 mL deionized water to form a gel. Then, 0.05 mol $Zn(Ac)_2{\cdot}2H_2O$ and 0.15 mol L-cysteine were added into the gelatin gel to form a viscous, homogeneous solution whose pH value was adjusted to 10.0 with ammonia. After 15 min of magnetic stirring, the solution was transferred into a Teflon-lined stainless steel autoclave of 50 mL capacity, sealed and maintained at 100 °C for 24 h. Finally, the product was filtered, washed with deionized water and desiccated at 60 °C. The thermal treatment of the ZnS-gelatin precursor for producing ZnO porous microspheres was performed in a furnace at 600 °C for 4–24 h under air atmosphere.

Crystallographic phase of the prepared samples were investigated by X-ray diffraction at room temperature with a German Bruker AXS D8 ADVANCE diffractometer using CuKα1 radiation (λ = 1.5405 Å). The accelerating voltage, emission current, and scanning speed were 40 kV, 40 mA and 0.2°/s, respectively. The morphologies and microstructures of the samples were observed using Tecnai-12 transmission electron microscope (TEM) with an accelerating voltage of 120 kV and a Hitachi S4800 field-emission scanning electron microscope (FE-SEM). The FTIR spectra were recorded on a Nicolet Fourier 5700 spectrometer in the range of 400–4000 cm^{-1} using KBr disks. N_2 adsorption measurement was carried out at 77 K on a micromeritics ASAP 2020 volumetric adsorption analyzer. Before the measurement, the samples were outgassed under vacuum at 90 °C for 5 h.

The photocatalytic measurements: the photocatalytic activity experiments on the obtained products for the decomposition of RB in air were performed at ambient temperature. In the typical experiment, 0.1 g sample was dispersed in 100 mL of RB solutions having a concentration of 1×10^{-5} M. Prior to irradiation, the suspensions were magnetically stirred in a dark condition for 15 min to establish adsorption/desorption equilibrium. The suspensions were then irradiated under the UV lamp at a 12 cm separation distance. A 400 W high-pressure Hg lamp (Institute of Electric Light Source, Beijing) with a maximum emission at about 365 nm was used as the light source. A light filter was placed in front of the reaction vessel to cut off the light longer than 480 nm and obtain UV light. Degradation was monitored by taking aliquots at given irradiation time intervals (10 min). The suspension including photocatalyst and RB were centrifuged and the absorption spectra of the samples were recorded by measuring the absorbance at 553 nm with UV–vis (Shimadzu UV–vis 3010) spectrometer. The concentrations of RB were calculated using the Beer–Lambert law $A = eCl$, where A is the absorbance at λ_{max} of RB, e is the molar absorptivity of RB ($79.5l \times 10^3$ L/mol com) [30] and l is the sample cell length (1 cm). RB degradation was expressed as C/C_0 vs. UV-irradiation time, where C_0 was the initial concentration.

3. Results and discussion

3.1. Synthesis and powder characterization of ZnS spheres

XRD patterns of the ZnS spheres synthesized at 100 °C for 3–24 h are shown in Fig. 1, it can be seen that the product initially formed at a reaction time of 3 h is an amorphous precursor (Fig. 1a). With the extension of the reaction time from 3–24 h, the as-obtained products gradually crystallized to hexagonal ZnS crystals (JCPDS card 80-0007). The size and morphology of these products were

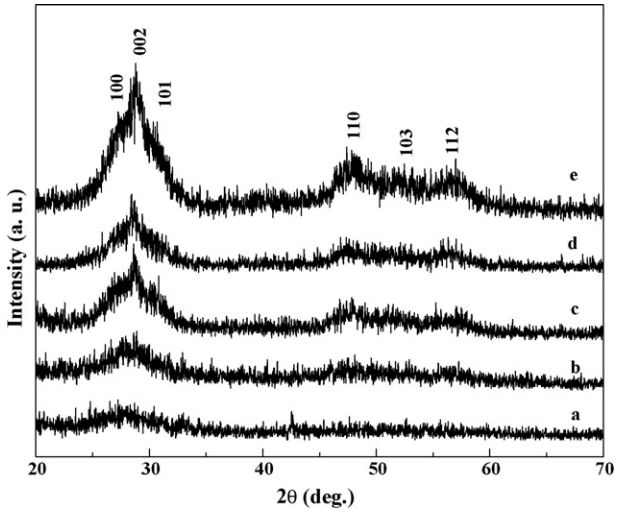

Fig. 1. XRD patterns of ZnS spheres synthesized at 100 °C for different duration time: (a) 3 h; (b) 4 h; (c) 6 h; (d) 12 h; (e) 24 h.

observed by TEM and the results were shown in Fig. 2. ZnS nanoparticles with the size of less than 10 nm are found at a reaction time of 3 h and Fig. 2a shows the corresponding TEM measurement. The XRD result (Fig. 1a) also proves that these products are amorphous. Then, as the reaction proceeds, the hexagonal ZnS is formed by crystallization. Fig. 2b shows the TEM image of the product obtained at 4 h, which reveals that lots of small nanocrystals with an average size of 40 nm and a few solid spheres coexist in the figure. It can also be observed that the nanocrystals do not disperse well but contact with each other which indicates a trend to assemble. The spheres accompanied with the nanocrystals can also confirm that some ZnS nanocrystals have self-assembled into ZnS spheres. As the reaction time prolonged from 6 h to 12 h (Fig. 2c and d), the spheres subsequently increased in quantity and meanwhile the nanoparticles with an average size of 40 nm reduced in quantity. ZnS solid spheres with an average diameter of 570 nm were obtained as the reaction time increased to 24 h (Fig. 2e). From the TEM results, it can be deduced that ZnS primary nanocrystals with an average size of 40 nm were first formed, and as building blocks these nanocrystals then self-assembled to form 3D ZnS spheres. As shown in the FE-SEM image in Fig. 2f, the panoramic morphology of the as-obtained ZnS is spherical with average diameter of around 570 nm, which corresponds to the TEM results. From high magnified FE-SEM image, we can see the surfaces of spheres are constructed by nanoparticles as seen in Fig. 2g, which confirms the above discussion.

Gelatin is a denatured protein with high molecular weight and contains high concentrations of polypeptides (poly-L-aspartate and poly-L-glutamate) [31]. As gelatin molecules contain high concentrations of amido and carbonyl groups, they can covalently bind to the surface atoms of ZnS through coordination bond between carbonyl group and Zn^{2+} and form gelatin-stabilized ZnS crystals. Then gelatin macromolecules can restrain the growth of ZnS crystals effectively. In addition, gelatin-stabilized ZnS nanocrystals can cross-link together via hydrogen bonds interactions formed by amido groups between gelatin molecules [32]. If gelatin is not used, only small near spherical aggregates with rough surface and loose structure are obtained (as shown in Fig. 3a and b). This can be attributed to the inadequate coordination and weak hydrogen interactions between excessive L-cysteine molecules. But once the gelatin was added into the solution, large spheres with smooth surface can be obtained (Fig. 2f and g). Therefore, in this work, stable complex formed in solution first between Zn^{2+} and –SH in L-cysteine [33]. Then, as the reaction proceeded, the initial amor-

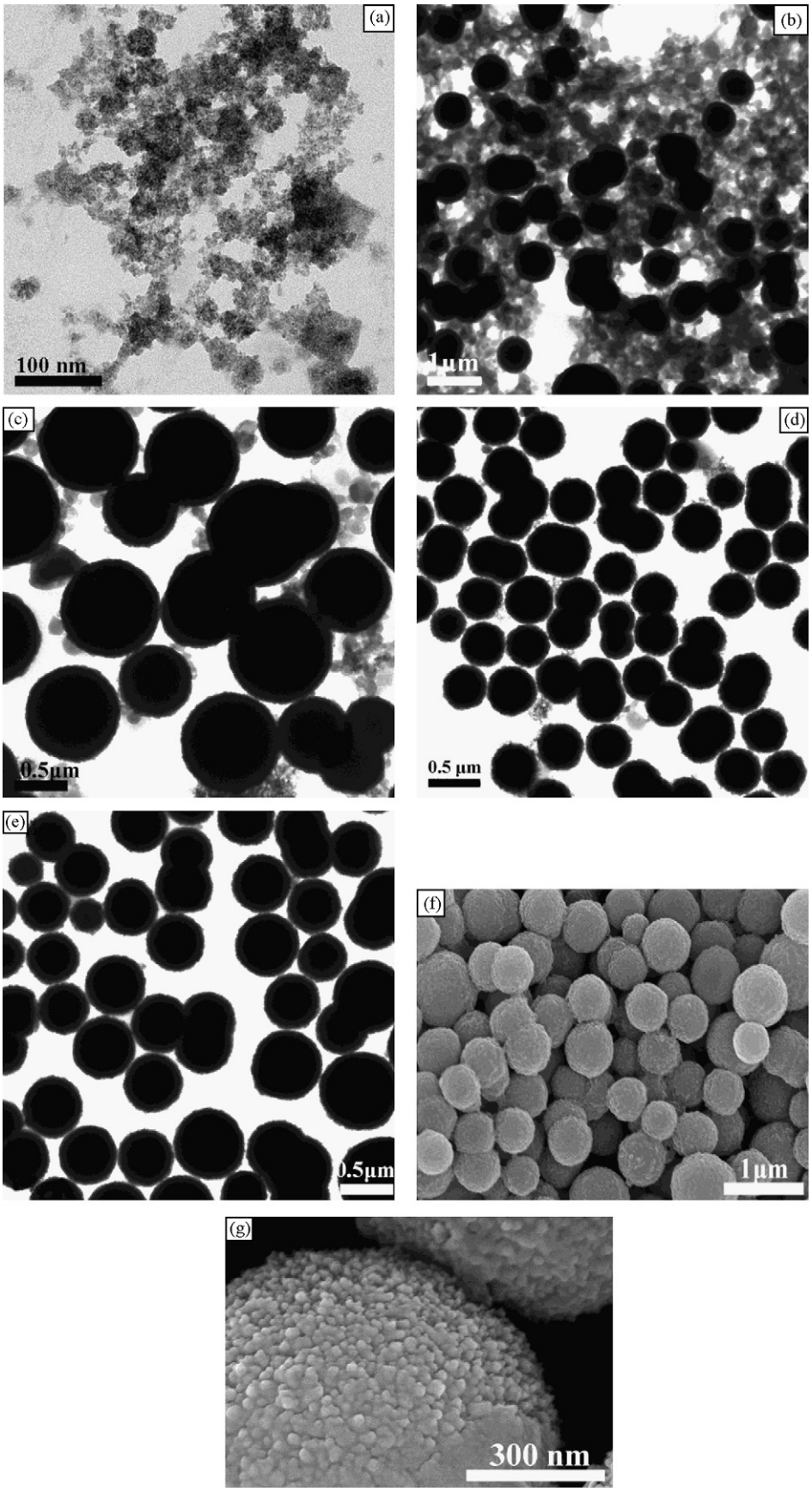

Fig. 2. TEM images of ZnS spheres synthesized at 100 °C for different duration time: (a) 3 h; (b) 4 h; (c) 6 h; (d) 12 h; (e) 24 h; (f) FE-SEM image of ZnS spheres; (g) high-magnification FE-SEM image of ZnS spheres.

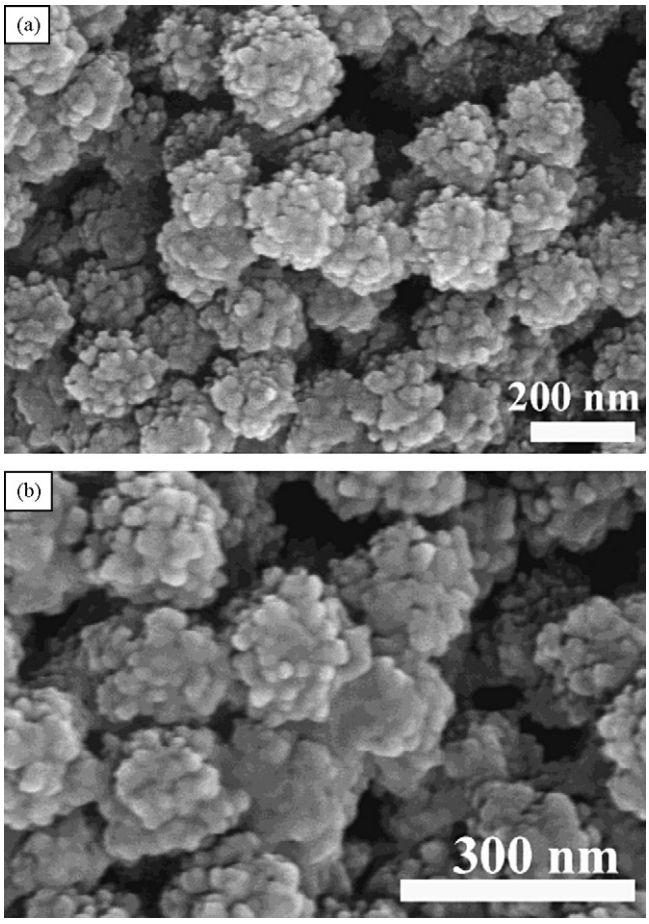

Fig. 3. Low and high-magnification FE-SEM images of ZnS synthesized without gelatin.

phous ZnS nuclei gradually crystallize and simultaneously, gelatin molecules covalently bind to the surface atoms of ZnS and form gelatin-stabilized ZnS powders. The gelatin-stabilized ZnS powders then self-assembled homogeneously to form 3D spheres through hydrogen bonds interactions formed by amido groups between gelatin molecules.

3.2. Conversion of ZnS spheres to ZnO porous spheres

The XRD pattern (Fig. 4) shows the thermal treatment of the ZnS spheres in an air atmosphere at different temperature for 4 h. It can be seen that when ZnS spheres were annealed at 400 °C, the as-obtained product is still ZnS phase (Fig. 4b). As increase the temperature to 500 °C (Fig. 4c) and 600 °C (Fig. 4d), the corresponding XRD peaks confirm that the products are pure hexagonal ZnO phase (JCPDS card No. 36-1451). The sharper XRD peaks of the products after thermal treatment indicate a better crystallinity compared to ZnS crystals.

The FTIR spectra demonstrate the chemical nature of the ZnS Fig. 5a and ZnO products obtained by thermal treatment of ZnS at 500 °C (Fig. 5b) and 600 °C (Fig. 5c) for 4 h, respectively. The adsorption peaks at ca. 1600, 1505, 1224 cm^{-1} in Fig. 5a are the characteristic vibrations of acylamino bonding of gelatin. The vibration band of $(COO)^-$ at ca. 1390 cm^{-1} also indicate the existence of amino acid [34]. The broad band at 3400 cm^{-1} can be attributed to the O–H stretching mode of the adsorbed and interlamellar water molecules. So, it can be deduced the presence of gelatin in ZnS spheres from Fig. 5a. In Fig. 5b, the vibration band of NH at ca. 1600 cm^{-1} and vibration band of $(COO)^-$ at ca. 1390 cm^{-1} indicate

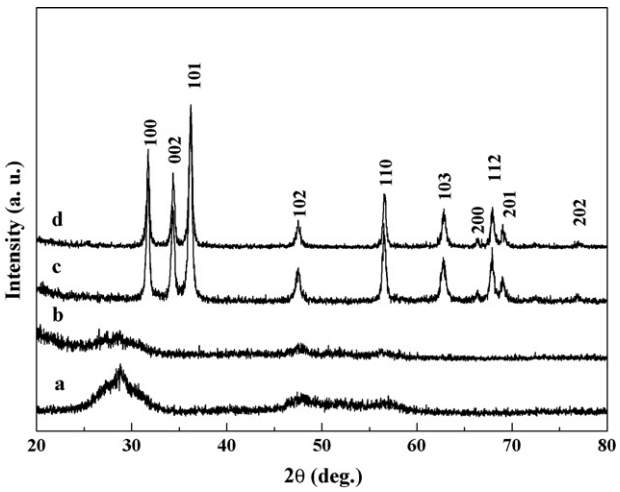

Fig. 4. XRD patterns of ZnS spheres (a) and the products obtained by annealing ZnS spheres at different temperature for 4 h: (b) 400 °C; (c) 500 °C; (d) 600 °C.

that there are still some organic materials in ZnO particles obtained at 500 °C for 4 h, which means an inadequate decomposition of gelatin. When ZnS particles were annealed at 600 °C for 4 h, the FTIR spectrum of the as-obtained ZnO (Fig. 5c) is very similar with that of commercial ZnO particles (Fig. 5d), indicating that gelatin has been decomposed completely at 600 °C for 4 h. The broad peak at 3440 cm^{-1} and the small peak at 1630 cm^{-1} are assigned to the hydroxyl groups of chemisorbed and/or physisorbed H_2O molecules on the ZnO surface. The FTIR results confirm that 600 °C is an appropriate annealing temperature.

Fig. 6 shows the XRD patterns of ZnO products obtained by thermal treatment of ZnS spheres at 600 °C for different time. It can be seen that all the products are pure hexagonal ZnO phase with sharp XRD peaks which indicate a well crystallinity. No obvious differences in XRD patterns can be observed from Fig. 6.

The morphology of ZnO obtained by thermal treatment of ZnS spheres at 600 °C for different time were observed by FE-SEM and TEM, and the results were shown in Figs. 7 and 8. When the annealing time is 2 h, FE-SEM image (Fig. 7a) shows that the morphology of the as-obtained ZnO crystals are still solid spheres with an average of around 500 nm. It can be observed from TEM image (Fig. 8a) that the surface of ZnO spheres are rough which can be attributed to the decomposition of gelatin on the surface of the spheres. As

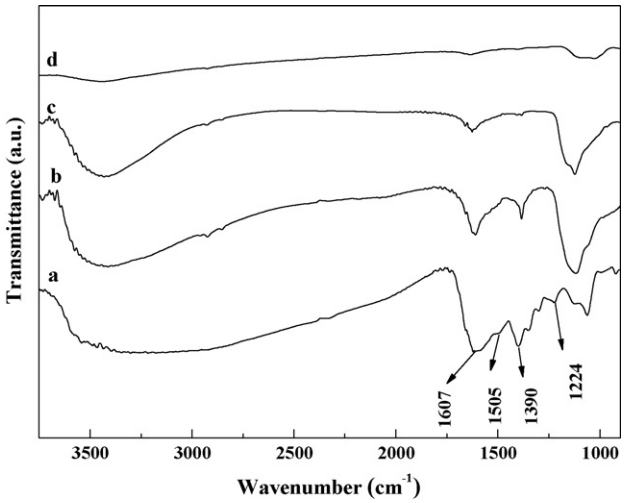

Fig. 5. FTIR spectra of the products: (a) ZnS spheres; (b) ZnO synthesized at 500 °C for 4 h; (c) ZnO synthesized at 600 °C for 4 h; (d) commercial ZnO particles.

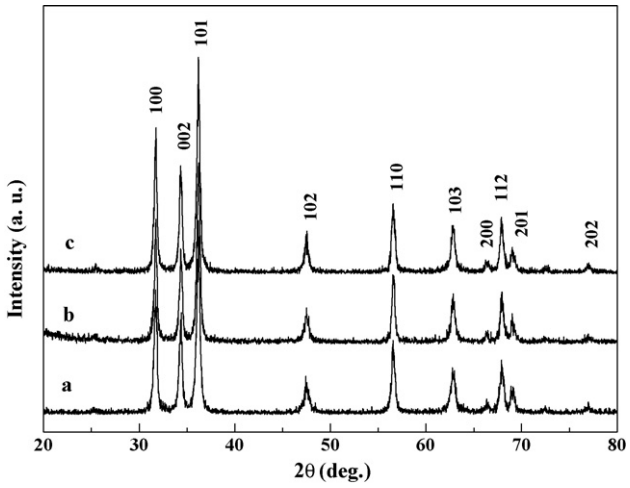

Fig. 6. XRD patterns of ZnO synthesized by annealing ZnS at 600 °C for different time: (a) 2 h; (b) 4 h; (c) 24 h.

increase the annealing time to 4 h, the ZnO crystal is still spherical with an average size of around 500 nm (Fig. 7b). But it can also be clearly observed that the ZnO spheres are composed of small nanocrystals with disordered pores exist among them. TEM image (Fig. 8b) shows that these pores not only exist among the surface nanoparticles but also within the ZnO spheres. Therefore, ZnO porous spheres can be easily synthesized by thermal treatment of ZnS spheres in air at 600 °C for 4 h. When the annealing time was prolonged to 24 h, the FE-SEM (Fig. 7c) and TEM (Fig. 8c) images reveal that the morphology of the ZnO is still porous sphere which is almost the same as ZnO crystals obtained at 600 °C for 4 h, only a few nanocrystals break off from ZnO spheres during the annealing process, which indicates the well stability of the ZnO porous structures. From the FE-SEM and TEM results, it can be concluded that during the annealing progress, ZnS nanoparticles can be oxidized to ZnO nanoparticles with the assisted of O_2, and the porous structure of ZnO spheres can be obtained because of the decomposition of gelatin molecules among ZnS primary nanoparticles.

The porosity of ZnS spheres and porous ZnO spheres was determined by N_2 adsorption by BET (Brunauer–Emmett–Teller) measurements. N_2 adsorption–desorption isotherm and the pore size distribution curve (insert) for ZnS spheres and porous ZnO spheres are shown in Fig. 9. For ZnS spheres, the BET surface area is about 8.21 m^2/g and the BJH (Barret–Joyner–Halenda) average pore diameter is about 12 nm. While for porous ZnO spheres, the BET surface area increases to about 27.58 m^2/g and the BJH average pore diameter increases to about 45 nm. Furthermore, ZnS spheres and ZnO porous spheres show a similar N_2 adsorption and desorption isotherm corresponding to type V isotherm with a H1 hysteresis loop, but the N_2 adsorption quantity for porous ZnO spheres is much higher than that of ZnS spheres, indicating the abundance of mesopores in porous ZnO spheres, which is in good agreement with those observed in FE-SEM and TEM images. So, it can be concluded that gelatin decomposition improves the porous structure of the products. The data implies that the as-obtained porous ZnO can be potentially applied in adsorption and various catalytic reactions, such as in the removal of heavy metal ions and other pollutant as in water treatment [35].

3.3. Photocatalytic activity studies

ZnS and ZnO all have been used as a semiconductor-type photocatalyst for the photoreductive dehalogenation of halogenated benzene derivatives, photocatalytic degradation of water pollutants and photocatalytic reduction of toxic metal ions. So we investigated photocatalytic activity of ZnS spheres and ZnO porous spheres with the photocatalytic degradation of RB as a test reaction. The characteristic absorption of RB at 553 nm was chosen as the monitored parameter for the photocatalytic degradation process. Fig. 10 shows the evolution of RB absorption spectra in the presence of 0.1 g of ZnS spheres (Fig. 10a) and 0.1 g of ZnO porous spheres obtained by annealing of ZnS spheres at 600 °C for 4 h (Fig. 10b). From Fig. 10 we can see the intensity of the adsorption peaks corresponding to RB diminish gradually as the exposure time increases. The slight blue-shift of absorption peaks as the increase of exposure time could be attributed to a de-ethylated process of RB in a

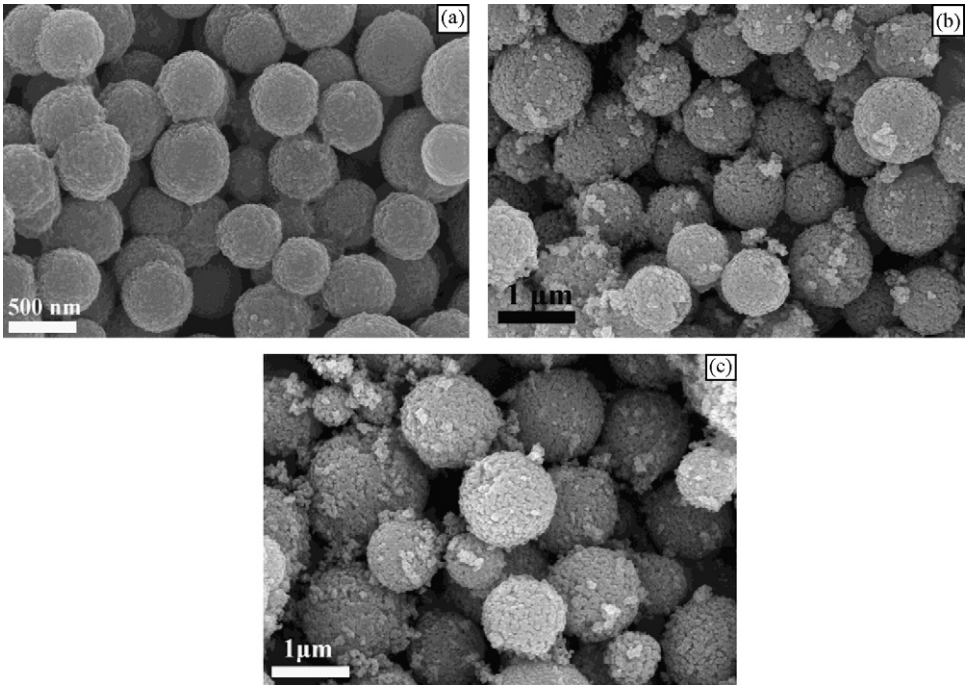

Fig. 7. FE-SEM images of ZnO synthesized by annealing ZnS at 600 °C for different time: (a) 2 h; (b) 4 h; (c) 24 h.

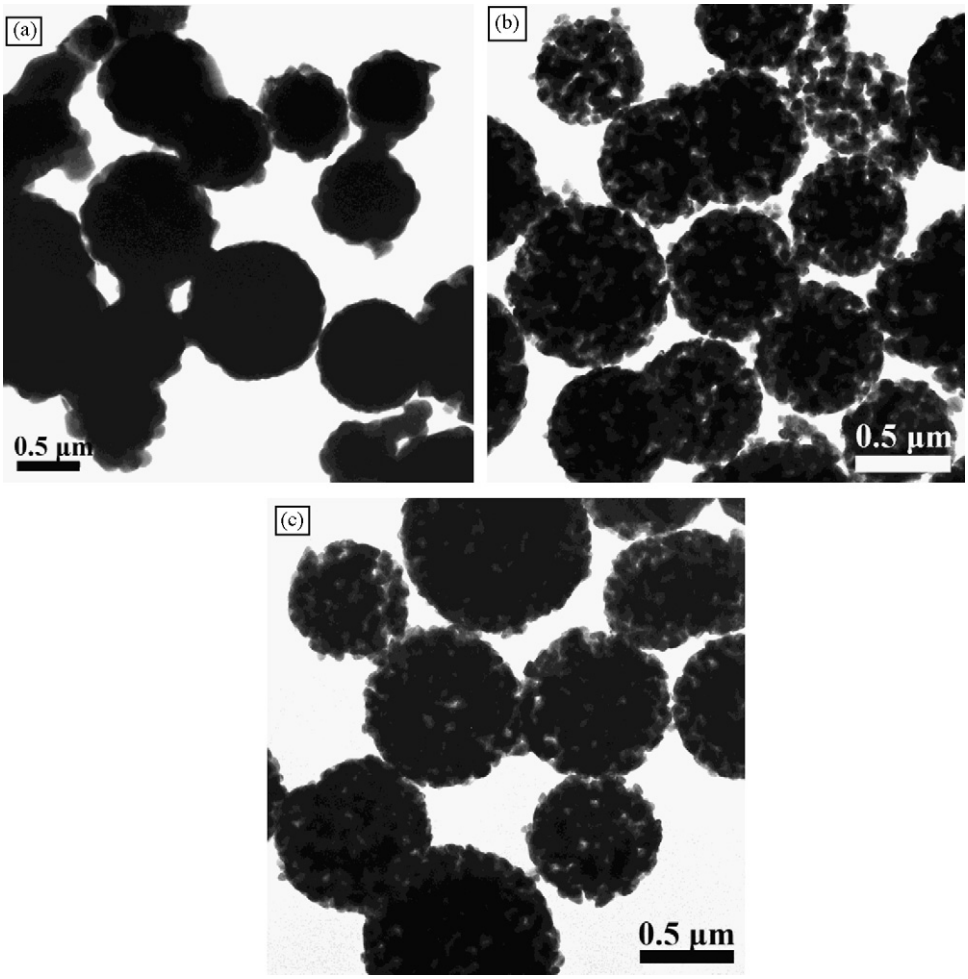

Fig. 8. TEM images of ZnO synthesized by annealing ZnS at 600 °C for different time: (a) 2 h; (b) 4 h; (c) 24 h.

stepwise manner [36]. No new absorption peaks appeared in either the visible or ultraviolet regions, which indicated the effective photodegradation of RB.

Comparative experiments were carried out to investigate the photocatalytic activity of the products. The solution of RB was subjected to a series of experimental conditions and the results were shown in Fig. 11. The photocatalytic effect on the solution degradation without catalysts but under exposure to UV light (Fig. 11a) is almost the same as that with ZnO porous spheres but no exposure to UV light (Fig. 11b), only a slight decrease in the concentration of RB is detected. However, gelatin – assist – synthesized ZnS spheres (Fig. 11c) show very high photocatalytic activity. After 60 min, the decolourization degree of RB solution containing ZnS spheres is near to 100%, which is similar to Degussa P25 TiO_2 (Fig. 11f). The porous ZnO spheres obtained by annealing ZnS at 600 °C for 4 h (Fig. 11d) and 24 h (Fig. 11e) show a higher photocatalytic performance compared to ZnS spheres and Degussa P25 TiO_2, the decolourization degree of RB solution reaches to almost 100% after 40 min of irradiation which may be because of their porous structure and high BET surface area. As we have known that materials with porous structure have better adsorption ability than materials without porous structure, the dye molecules, H_2O, OH^-, O_2 and radicals ($OH^\bullet$, $O_2^{-\bullet}$, $HO_2^\bullet$) generated by them are adsorbed on their surface efficiently and the whole photocatalytic process are promoted greatly. So the materials with porous structure usually show better photocatalytic performance compared to the materials without porous structure. Furthermore, a large surface area can produce more active center of reaction to promote the rate of a photocatalytic reaction [37]. It is another reason for the higher photocatalytic ability of porous ZnO spheres

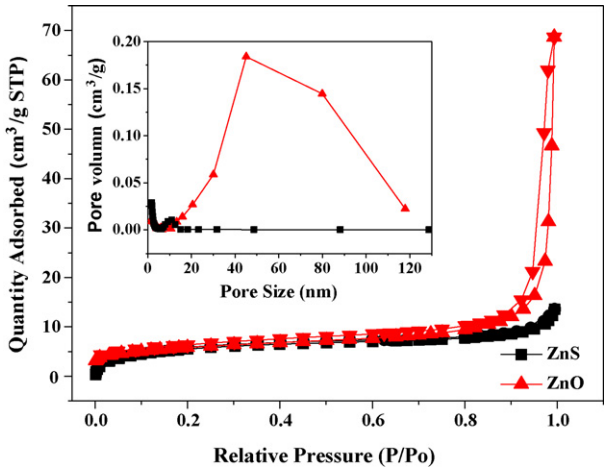

Fig. 9. Nitrogen adsorption/desorption isotherm and Barrett–Joyner–Halenda (BJH) pore size distribution plot (inset) of ZnS spheres and ZnO porous spheres.

The stability of a photocatalyst is very important for industrial application. Thus, in this experiment, ZnO porous spheres were recycled after bleaching the RB under UV light-irradiation and were reused five times in the decomposition of RB to test the chemical stability (Fig. 12). After five recycles for the photodegradation

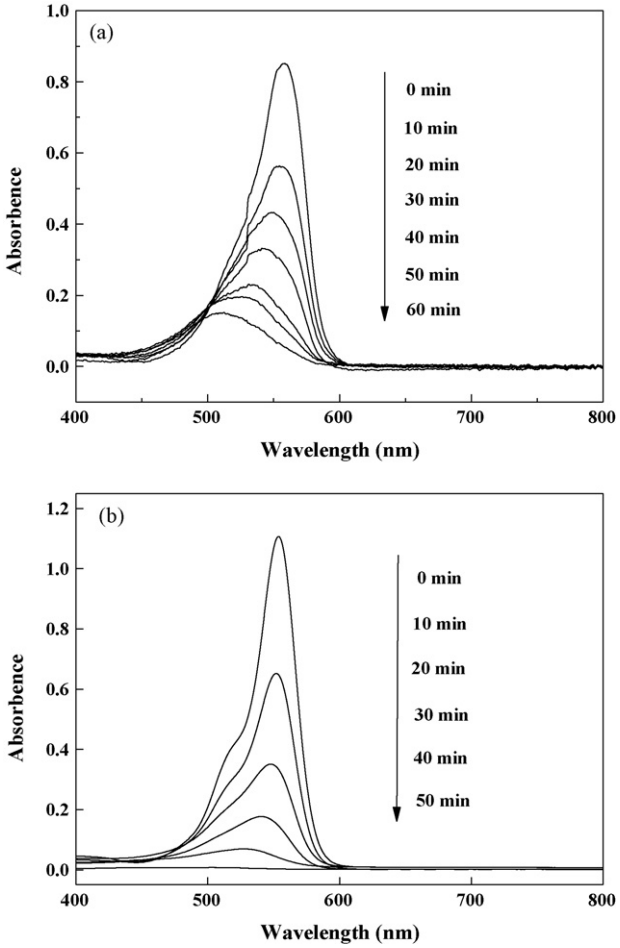

Fig. 10. Absorption spectrum of a solution of RB in the presence of ZnS spheres (a) and ZnO porous spheres (b) under exposure to UV light.

of RB, the catalyst did not exhibit obvious loss of activity which indicated a high stability of ZnO porous spheres in photocatalytic reaction. Moreover, XRD was also performed to confirm the chemical stability of ZnO porous spheres (not shown here), the results of the sample after the fifth run was almost similar to that of the

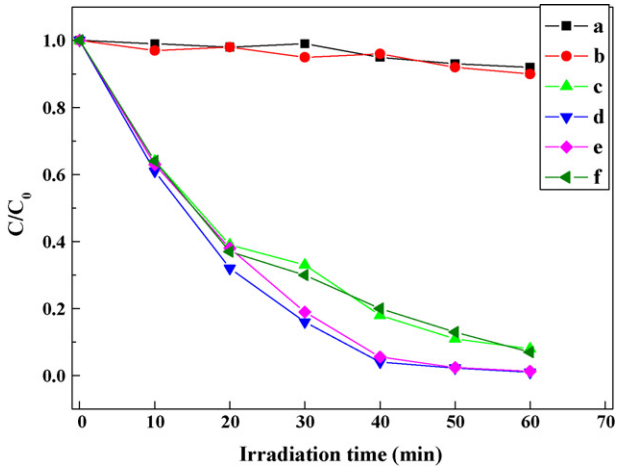

Fig. 11. Photodegradation of RB under different conditions: (a) without catalyst, with UV light (blank); (b) with 3D ZnO porous spheres in the dark; (c) with 3D ZnS pheres under UV-irradiation; (d) with 3D ZnO porous spheres synthesized at 600 °C for 4 h; (e) with 3D ZnO porous spheres synthesized at 600 °C for 24 h; (f) with Degussa P25 TiO_2 under UV-irradiation.

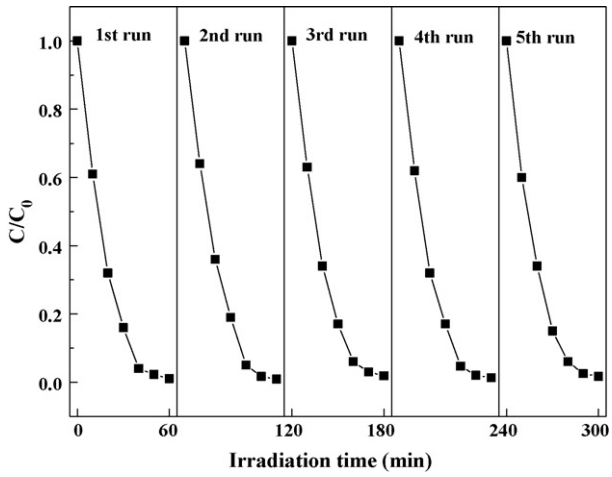

Fig. 12. Cycling runs in the photocatalytic degradation of RB in the presence of ZnO porous spheres under UV light-irradiation.

as-prepared fresh sample, and they were in good agreement with hexagonal ZnO. Both XRD patterns and recycled experiment support the conclusion that the as-obtained ZnO porous spheres are very stable during photocatalytic process.

4. Conclusion

In summary, 3D porous ZnO microspheres had been synthesized by thermal treatment of ZnS microspheres under air atmosphere at 600 °C for 4–24 h. The ZnS monodisperse spheres were synthesized via the reaction of $Zn(Ac)_2$ and L-cysteine with the assisted of gelatin. The as-obtained ZnO porous spheres contained pores with an average diameter of ~45 nm and a specific surface area of 27.58 m^2/g. They displayed better photocatalytic activity compared with ZnS microspheres and Degussa P25 TiO_2 powders by the photodegradation of RB at ambient temperature. This is because of their porous structure and high BET surface area. This simple, environmentally benign, and inexpensive bio-assisted route can also be extend to the preparation of the other metal chalcogenides including FeS, CuS, NiS, PbS, MnS and CoS nanostructures which could act as unique precursors for templating synthesis of a variety of metal oxide including Fe_2O_3, CuO, NiO, PbO, Mn_2O_3 and Co_2O_3.

Acknowledgement

This work is supported by the Natural Science Foundation of Beijing (No. 4082008), Scientific and Technological Development Project of Beijing Education Committee (No. KM200710005029), and the Opening Project of State Key Laboratory of Green Building Materials (No. GBM-08-KF104).

References

[1] L.L. Welbes, A.S. Borovik, Confinement of metal complexes within porous hosts: development of functional materials for gas binding and catalysis, Acc. Chem. Res. 38 (2005) 765–774.
[2] C.J. Martinez, B. Hockey, C.B. Montgomery, S. Semncik, Porous tin oxide nanostructured microspheres for sensor applications, Langmuir 21 (2005) 7937–7944.
[3] L.L. Yang, Z.H. Yang, W.X. Cao, L. Chen, J. Xu, H.Z. Zhang, Luminescence 3D-ordered porous materials composed of CdSe and CdTe nanocrystals, J. Phys. Chem. B 109 (2005) 11501–11504.
[4] F. Fajula, A. Galarneau, F. Di Renzo, Advanced porous materials: new developments and emerging trends, Microporous Mesoporous Mater. 82 (2005) 227–239.
[5] U. Simon, M.E. Franke, Electrical properties of nanoscaled host/guest compounds, Microporous Mesoporous Mater. 41 (2000) 1–36.

[6] F. Xu, P. Zhang, A. Navrotsky, Z.Y. Yuan, T.Z. Ren, M. Halasa, B.L. Su, Hierarchically assembled porous ZnO nanoparticles: Synthesis, surface energy, and photocatalytic activity, Chem. Mater. 19 (2007) 5680–5686.
[7] G.W. Nyce, J.R. Hayes, A.V. Hamza, J.H. Satcher, Synthesis and characterization of hierarchical porous gold materials, Chem. Mater. 19 (2007) 344–346.
[8] H.F. Zhang, J. Long, A.I. Cooper, Aligned porous materials by directional freezing of solutions in liquid CO_2, J. Am. Chem. Soc. 127 (2005) 13482–13483.
[9] W.H. Suh, K.S. Suslick, Magnetic and porous nanospheres from ultrasonic spray pyrolysis, J. Am. Chem. Soc. 127 (2005) 12007–12010.
[10] I.I. Slowing, B.G. Trewyn, S. Giri, V.S.Y. Lin, Mesoporous silica nanoparticles for drug delivery and biosensing applications, Adv. Funct. Mater. 17 (2007) 1225–1236.
[11] H.M. Chen, J.H. He, H.M. Tang, C.X. Yan, Porous silica nanocapsules and nanospheres: dynamic self-assembly synthesis and application in controlled release, Chem. Mater. 20 (2008) 5894–5900.
[12] Z.Y. Fan, J.G. Lu, Zinc oxide nanostructures: synthesis and properties, J. Nanosci. Nanotechnol. 5 (2005) 1561–1573.
[13] M.H. Huang, S. Mao, H. Feick, H.Q. Yan, Y.Y. Wu, H. Kind, E. Wdber, R. Russo, P.D. Yang, Room temperature ultraviolet nanowire nanolasers, Science 292 (2001) 1897–1899.
[14] J. Schrier, D.O. Demchemko, L.W. Wang, Optical properties of ZnO/ZnS and ZnO/ZnTe heterostructures for photovoltaic applications, Nano. Lett. 7 (2007) 2377–2382.
[15] N. Tian, Z.Y. Zhou, S.G. Sun, Y. Ding, Z.L. Wang, Synthesis of tetrahexahedral platinum nanocrystals with high-index facets and high electro-oxidation activity, Science 316 (2007) 732–735.
[16] R. Li, S. Yabe, M. Yamashita, UV-shielding properties of zinc oxide-doped ceria fine powders derived via soft solution chemical routes, Mater. Chem. Phys. 75 (2002) 39–44.
[17] K. Nomura, H. Ohta, K. Ueda, Thin-film transistor fabricated in single-crystalline transparent oxide semiconductor, Science 300 (2003) 1269–1272.
[18] S.H. Jo, J.Y. Lao, Z.F. Ren, Field-emission studies on thin films of zinc oxide nanowires, Appl. Phys. Lett. 83 (2003) 4821–4823.
[19] Y.F. Qiu, S.H. Yang, ZnO nanotetrapods: controlled vapor-phase synthesis and application for humidity sensing, Adv. Funct. Mater. 17 (2007) 1345–1352.
[20] C. Ye, Y. Bando, G. Shen, D. Golberg, Thickness-dependent photocatalytic performance of ZnO nanoplatelets, J. Phys. Chem. B 110 (2006) 15146–15151.
[21] M. Mo, J.C. Yu, L.Z. Zhang, S.K. Li, Self-assembly of ZnO nanorods and nanosheets into hollow microhemispheres and microspheres, Adv. Mater. 17 (2005) 756–760.
[22] Z.H. Dai, K. Liu, Y.W. Tang, X.D. Yng, J.C. Bao, J. Shen, A novel tetragonal pyramid-shaped porous ZnO nanostructure and its application in the biosensing of horseradish peroxidase, J. Mater. Chem. 18 (2008) 1919–1926.
[23] H.Q. Wang, G.H. Li, L.C. Jia, G.Z. Wang, C.J. Tang, Controllable preferential-etching synthesis and photocatalytic activity of porous ZnO nanotubes, J. Phys. Chem. C 112 (2008) 11738–11743.
[24] P.X. Gao, Z.L. Wang, Mesoporous polyhedral cages and shells formed by textured self-assembly of ZnO nanocrystals, J. Am. Chem. Soc. 125 (2003) 11299–11305.
[25] B. Reeja-Jayan, E. De la Rosa, S. Sepulveda-Guzman, R.A. Rodriguez, M.J. Yacaman, Structural characterization and luminescence of porous single crystalline ZnO nanodisks with sponge-like morphology, J. Phys. Chem. C 112 (2008) 240–246.
[26] C.X. Shan, Z. Liu, Z.Z. Zhang, D.Z. Shen, S.K. Hark, A simple route to porous ZnO and ZnCdO nanowires, J. Phys. Chem. B 110 (2006) 11176–11179.
[27] Z. Gui, J. Liu, Z.Z. Wang, L. Song, Y. Hu, W.C. Fan, D.Y. Chen, From muticomponent precursor to nanoparticle nanoribbons of ZnO, J. Phys. Chem. B 109 (2005) 1113–1117.
[28] J.G. Yu, X.X. Yu, Hydrothermal synthesis and photocatalytic activity of zinc oxide hollow spheres, Environ. Sci. Technol. 42 (2008) 4902–4907.
[29] Q.Y. Li, E.B. Wang, S.H. Li, C.L. Wang, C.G. Tian, G.Y. Sun, J.M. Gu, R. Xu, Template-free polyoxometalate-assisted synthesis for ZnO hollow spheres, J. Solid State Chem. 182 (2009) 1149–1155.
[30] M. Srinivasan, T. White, Degradation of methylene blue by three-dimensionally ordered macroporous titania, Environ. Sci. Technol. 41 (2007) 4405–4409.
[31] J. Zhan, H.P. Lin, C.Y. Mou, Biomimetic formation of porous single crystalline $CaCO_3$ via nanocrystal aggregation, Adv. Mater. 15 (2003) 621–623.
[32] Q. Wu, H. Cao, S. Zhang, X. Zhang, D. Rabinovich, Generation and optical properties of monodisperse Wurtzite-type ZnS microspheres, Inorg. Chem. 45 (2006) 7316–7322.
[33] W. Bae, R.K. Mehra, Cysteine-capped ZnS nanocrystallites: Preparation and characterization, J. Inorg. Biochem. 70 (1998) 125–135.
[34] J.A. Dean, Lange's Handbook of Chemistry, 15th ed., McGrawHill, New York, 2003.
[35] M. Kurtz, J. Strunk, O. Hinrichsen, M. Muhler, K. Fink, B. Meyer, C. Woell, Active sites on oxide surfaces: ZnO-catalyzed synthesis of methanol from CO and H_2, Angew. Chem., Int. Ed. 44 (2005) 2790–2794.
[36] T. Watanabe, T. Takizawa, K. Honda, Photo-catalysis through excitation of adsorbates. 1. Highly efficient *N*-deethylation of Rhodamine B adsorbed to CDS, J. Phys. Chem. 81 (1977) 1845–1851.
[37] Y. Zhao, X. Zhang, J. Zhai, J. He, L. Jiang, Z. Liu, S. Nishimoto, T. Murakami, A. Fjuishima, D. Zhu, Enhanced photocatalytic activity of hierarchically micro-/nano-porous TiO_2 films, Appl. Catal. B: Environ. 83 (2008) 24–29.